

Article

Improvement of PM_{2.5} Forecast in China by Ground-Based Multi-Pollutant Emission Source Inversion in 2022

Lili Zhu ^{1,2,3}, Xiao Tang ⁴, Wenyi Yang ⁵, Yao Zhao ⁶, Lei Kong ⁴, Huangjian Wu ⁴, Meng Fan ¹ , Chao Yu ¹ 
and Liangfu Chen ^{1,*}

- ¹ Aerospace Information Research Institute, Chinese Academy of Sciences, No.9 Dengzhuang South Road, Haidian District, Beijing 100094, China; zhull@radi.ac.cn (L.Z.)
- ² University of Chinese Academy of Sciences, No.1 Yanqihu East Rd, Huairou District, Beijing 101408, China
- ³ China National Environmental Monitoring Centre, No.8-2 Anwai Dayangfang, Chaoyang District, Beijing 100012, China
- ⁴ Institute of Atmospheric Physics, Chinese Academy of Sciences, No.81 Beichen West Road, Chaoyang District, Beijing 100029, China
- ⁵ Center of Air Quality Simulation and System Analysis, Chinese Academy of Environmental Planning, Beijing 100041, China
- ⁶ 3Clear Technology Co., Ltd. 11/F, Block G, No. 7, Beitucheng West Road, Chaoyang District, Beijing 100029, China
- * Correspondence: chenlf@radi.ac.cn

Abstract: This study employs an ensemble Kalman filter assimilation method to validate and update the pollutant emission inventory to mitigate the impact of uncertainties on the forecasting performance of air quality numerical models. Based on nationwide ground-level pollutant monitoring data in China, the emission inventory for the entire country was inverted hourly in 2022. The emission rates for PM_{2.5}, CO, NO_x, SO₂, NMVOCs, BC, and OC updated by the inversion were determined to be 6.6, 702.4, 37.2, 13.4, 40.3, 3, and 18.2 ng/s/m², respectively. When utilizing the inverted inventory instead of the priori inventory, the average accuracy of all cities' PM_{2.5} forecasts was improved by 1.5–4.2%, especially for a 7% increase on polluted days. The improvement was particularly remarkable in the periods of January–March and November–December, with notable increases in the forecast accuracy of 12.5%, 12%, and 6.8% for the Northwest, Northeast, and North China regions, respectively. The concentration values and spatial distribution of PM_{2.5} both became more reasonable after the update. Significant improvements were particularly observed in the Northwest region, where the forecast accuracy for all preceding days was improved by approximately 15%. Additionally, the underestimated concentration of PM_{2.5} in the priori inventory compared to the observation value was notably alleviated by the application of the inversion.

Keywords: emission inventory; numerical forecasting; inventory inversion; forecast evaluation



Citation: Zhu, L.; Tang, X.; Yang, W.; Zhao, Y.; Kong, L.; Wu, H.; Fan, M.; Yu, C.; Chen, L. Improvement of PM_{2.5} Forecast in China by Ground-Based Multi-Pollutant Emission Source Inversion in 2022. *Atmosphere* **2024**, *15*, 181. <https://doi.org/10.3390/atmos15020181>

Academic Editor: Xiao-San Luo

Received: 3 January 2024

Revised: 22 January 2024

Accepted: 24 January 2024

Published: 31 January 2024



Copyright: © 2024 by the authors. Licensee MDPI, Basel, Switzerland. This article is an open access article distributed under the terms and conditions of the Creative Commons Attribution (CC BY) license (<https://creativecommons.org/licenses/by/4.0/>).

1. Introduction

Since the issuance of the “Action Plan for Air Pollution Prevention and Control” in 2013, China has established a series of strict emission standards and adopted several pollution control measures. Particularly, the implementation of dust removal, desulfurization, and denitrification measures in power plants and industrial boilers has achieved significant success in pollution control. Despite the achievements of the control measures, the occurrence of PM_{2.5} pollution during the winter season remains. Thus, the forecast accuracy of PM_{2.5} is crucial for control decision-making. Numerical simulation techniques for air quality have been improved and widely used in various fields, such as air quality forecasting and pollution source analysis. These techniques serve as important foundations and technical tools for PM_{2.5} pollution control and precise regulation [1].

The surface pollution source emission inventory is the fundamental input for air quality numerical models [2] and the quality of the emission inventory is identified as

one of the key factors influencing model performance [3–5]. Currently, there are significant differences among various emission inventories [6,7], and the use of different pollution emission inventories has a substantial impact on the simulation results of pollutant concentrations, especially for PM_{2.5} [8]. Emission inventories created using the traditional bottom-up approach are based on various statistical data. These inventories generally lag by more than 1 year due to slow data updates. In recent years, China's intensive control measures have led to rapid and dynamic changes in regional and urban atmospheric pollution sources, and the database obtained from the traditional emission inventories has considerable bias due to the limitation of updating speed. Therefore, Miyazaki K [9] utilized numerical assimilation based on observational data to invert and update pollution emission inventories, obtaining inventories with higher spatial and temporal resolution.

Several studies have been conducted to further enhance the forecasting performance of the numerical model. Peng Z et al. [10] employed data assimilation to validate and update pollution source emission inventories, and Feng S et al. [11] improved PM_{2.5} simulation by enhancing the initial conditions. However, neither of these studies conducted forecast verification experiments. Wu et al. [12] employed the ensemble Kalman filter (EnKF) assimilation method to establish a dynamic updating system for the inversion of multiple pollutant emission based on ground-level monitoring, resulting in improved forecasting performance for various pollutants over the next 7 days.

In this work, we further analyze the improvement performance and applicability of the inventory inversion system in PM_{2.5} forecasting for 2022. The concentration of key precursors and important components of PM_{2.5} (PM_{2.5}, CO, NO_x, SO₂, NMVOCs, BC, and OC, etc.) were inverted and verified based on traditional emission inventories using ground-level pollutant monitoring data. Forecast experiments were conducted for the next 9 days using both the a priori inventory and the inverted inventory. The PM_{2.5} forecast accuracy for the entire country and various regions was analyzed for the whole year, each month, polluted days, and the heating season. A comprehensive analysis of the improvement performance of the inverted inventory on short-term PM_{2.5} forecasting during typical pollution episodes was also conducted, along with a discussion of the current shortcomings.

2. Materials and Methods

2.1. Inventory Update

This study utilized an inversion system based on the EnKF method to update the emission source inventory. Comparative forecasting experiments were conducted using both the priori source inventory and the inverted source inventory to assess the impact of the updated inventory on PM_{2.5} forecasting performance (See Figure 1). The process involved randomly drawing a finite sample of ensemble perturbations based on the error statistics of the priori inventory. Then, these perturbations were added to the priori inventory to generate a short-term ensemble forecast to estimate the forecast error covariance matrix. The matrix was subsequently used to update the priori emission inventory, along with the observation and its error matrix.

Priori Inventory: The anthropogenic emission inventory for China is the gridded pollution source inventory MEIC [13–15], which was established by Tsinghua University for air quality models. The inventory has a reference year of 2019, with a spatial resolution of approximately 0.25° × 0.25°, covering 10 major atmospheric pollutants and greenhouse gases (SO₂, NO_x, CO, NMVOC, NH₃, CO₂, PM_{2.5}, PM₁₀, BC, and OC), including over 700 types of anthropogenic emission sources. Within the simulated region, the anthropogenic emission inventory for sources from outside China is MIX [16], with a reference year of 2019.

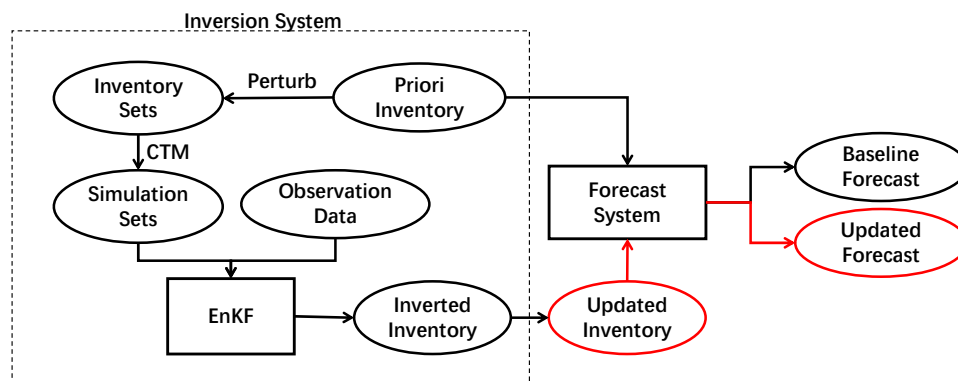


Figure 1. The forecasting experiment framework with the inversion update of the emission source inventory.

Emission Perturbation: Perturbations are applied to the major pollutants, such as SO_2 , NO_x , CO , NMVOC , NH_3 , $\text{PM}_{2.5}$, BC , and OC , based on their uncertainties [17,18]. Considering the trade-off between the approximation accuracy of the error covariance matrix and computational cost, the ensemble sample size is set to 50. The perturbed emission sources are represented in Equation (1):

$$E_i = E_0 \cdot \beta_i, \quad i = 1, 2, \dots, 50 \quad (1)$$

E_i represents the perturbation sample for the i th emission source, E_0 represents the priori emission source, and β_i is the perturbation coefficient of the i th emission source perturbation sample. Assuming that the error of the priori emission source follows a Gaussian distribution, β follows a Gaussian distribution with a mean value of 1 and a standard deviation corresponding to the Gaussian distribution of the emission source inventory uncertainty. Using the method proposed by Evensen G. [19], 50 spatially smoothed perturbation samples are extracted to perturb the emission sources. This results in a number of 50 perturbed emission source sample sets, which are then input into an atmospheric chemical transport model for simulation calculations.

Chemical Transport Model (CTM): This paper employs the Nested Air Quality Prediction Modeling System (NAQPMS), a three-dimensional Eulerian chemical transport model developed independently by the Institute of Atmospheric Physics, Chinese Academy of Sciences [20]. The simulation domain of the NAQPMS model covers an area between 70°E and 140°E in longitude and 15°N and 55°N in latitude, with a horizontal grid spacing of 15 km. This model utilizes a Sigma-Z terrain-following coordinate system with the vertical direction unevenly divided into 12 layers. The near-surface center height is approximately 47 m, and the model's layer top altitude is set at 20 km. The dynamical forcing field for the NAQPMS model is provided by the mesoscale meteorological model WRF (Weather Research and Forecasting Model). The version of WRF used in this study is WRF 3.5. The initial and boundary conditions for meteorological forecasts are derived from the Global Forecast System (GFS) data of the National Centers for Environmental Prediction (NCEP), with a temporal interval of 24 h, a spatial resolution of $0.5^\circ \times 0.5^\circ$, and a forecast lead time of 24 h.

EnKF: This paper employs the assimilation method of EnKF (Evensen G. 1994) for inventory inversion. The EnKF is a Monte Carlo approximation of the Kalman filter, where the initial uncertainty of state variables and model uncertainty are described by a set of random samples. Through Monte Carlo ensemble simulation, these errors can evolve in the model's dynamical system. All forecast errors are statistically derived from random

samples in the ensemble forecast. The error covariance matrix P can be estimated from simulation samples using Equation (2):

$$P = \frac{X'(X')^T}{N-1} \quad (2)$$

$X' = X - \bar{X}$, X represents the ensemble sample matrix, and \bar{X} represents the ensemble mean value. N represents the ensemble sample size, which is set to 50 in this case. According to Equation (2), the simulation error covariance matrix P_s and observation error covariance matrix P_o can be obtained separately. The ground-level pollutant monitoring data used in this paper are sourced from the China National Environmental Monitoring Center, including 1706 national monitoring stations (shown in Figure 2). The monitored pollutants comprise SO_2 , NO_2 , PM_{10} , CO , O_3 , and $\text{PM}_{2.5}$, with a temporal resolution of 1 h. Then, the assimilation analysis state (posteriori) X^a can be obtained according to Equation (3):

$$X^a = X^b + P_s H^T (H P_s H^T + P_o)^{-1} (D - H X^b) \quad (3)$$

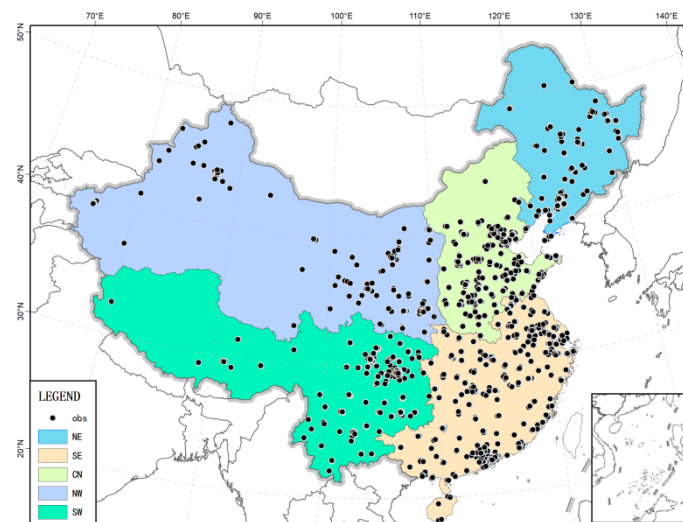


Figure 2. Distribution of monitoring stations and regional division in China.

X^b represents the augmented state of the background (priori); H is the linear observational operator; and D represents the vector of the observations with an error covariance matrix of P_o .

Forecast System: The same setting of which was used in the inversion system is applied to NAQPMS for forecasting. In order to validate the forecasting performance with the inversely updated emission, comparative experiments are conducted for $\text{PM}_{2.5}$ concentration forecasting using both the baseline emission inventory and the updated emission inventory. The baseline emission inventory is the priori inventory, while the updated inventory is obtained by calculating the average value of the inverted inventory for the preceding 7 days, with daily rolling updates. By inputting the priori inventory and the updated inventory, the forecast results for the baseline and updated inventory are obtained. The forecast system initiates daily at 20:00 (local time), projecting for the next 240 h. The forecast results for 5–28 h are labeled as 1 d, for 29–52 h as 2 d, etc.

2.2. $\text{PM}_{2.5}$ Forecast Evaluation

The $\text{PM}_{2.5}$ accuracy index is primarily used to evaluate the forecast accuracy. $\text{PM}_{2.5}$ forecast accuracy is defined as follows: If the actual $\text{PM}_{2.5}$ concentration falls within the $\pm 25\%$ range of the forecast value, then the $\text{PM}_{2.5}$ forecast is considered accurate. If the actual $\text{PM}_{2.5}$ concentration is above 25% of the forecast concentration, it is considered a low

forecast. If the opposite is true, it is considered a high forecast. The forecast accuracy rate (A) is calculated using Equation (4):

$$\text{Accuracy rate} = \frac{n}{N} \times 100\% \quad (4)$$

n represents the number of accurate days; N represents the total number of days.

In addition, statistical metrics such as the correlation coefficient (R), root mean square error (RMSE), and normalized mean bias (NMB) are also employed for the evaluation. In order to better characterize the PM_{2.5} forecasting performance across the country, the entire country is divided into five regions—Northeast (NE), North (NC), Southeast (SE), Northwest (NW), and Southwest China (SW)—which are based on administrative divisions and geographical locations (shown in Figure 2).

3. Results and Discussion

3.1. Analysis of Emission Inventory

Adjustments were made to the emission inventory of multiple pollutants nationwide using an inversion method. In the priori emission inventory, the emission rates for PM_{2.5}, CO, NO_x, SO₂, NMVOCs, BC, and OC across China in 2022 were 6.7, 297.3, 25.0, 16.3, 45.6, 2.8, and 5.6 ng/s/m², respectively. After inventory inversion, the emission rates became 6.6, 702.4, 37.2, 13.4, 40.3, 3.0, and 18.2 ng/s/m², respectively. Notably, PM_{2.5}, NMVOCs, and BC showed no significant changes for both methods. However, CO, NO_x, and OC were observed to increase by 136, 48, and 225%, respectively, while the SO₂ emission rate decreased by 18% after the inversion. Figure 3 shows the spatial distribution of CO, NO_x, OC, and SO₂ emission rates before and after the inversion. Most regions in China showed an increase in the CO emission rate. The NO_x emission rate in the NE, NC, and SE regions showed an overall decrease, especially in Beijing, Tianjin, Hebei, Shandong, Anhui, and Jiangsu provinces. However, in the NW and SW regions, there was an overall increase. OC showed an overall decrease in the SE, but a significant increase in the NE and NW regions. SO₂ emission rates increased in some provinces in the NE, NC, SE, and SW regions, with no significant adjustments in other regions.

The statistical results of pollutant emission rates in the NE, NC, SE, NW, and SW (shown in Table 1) showed significant adjustments after the inversion. In the NE region, CO, NO_x, and OC emission rates increased by 103, 36, and 157%, respectively. In the NC region, CO and OC were observed to undergo an increase of 80 and 73%, respectively, while SO₂ decreased by 23%. The SE region experienced a 128% increase in CO and a 22% decrease in SO₂ emission rates. The SW region had an increase of 118% in CO and 119% in NO_x, coupled with a 42% decrease in SO₂ emission rates. The NW region exhibited the most notable change in pollutant emission rates, where the PM_{2.5} emission rate increased by 231%, marking the most significant increase in PM_{2.5} emission rates among all regions. This could result from the absence of dust sources in the priori emission inventory, while the NW region is a major source of dust. Additionally, CO, NO_x, NMVOCs, BC, and OC emission rates in NW region also underwent substantial adjustments, with increases of 404, 214, 48, 150, and 414%, respectively. The reason for the significant adjustments in the Northwest region may be attributed to the incomplete pollution source statistical data in this area. Kong L et al. [21] also found that the basic pollution source statistical data in the NW region were relatively less, leading to more significant changes after the inversion.

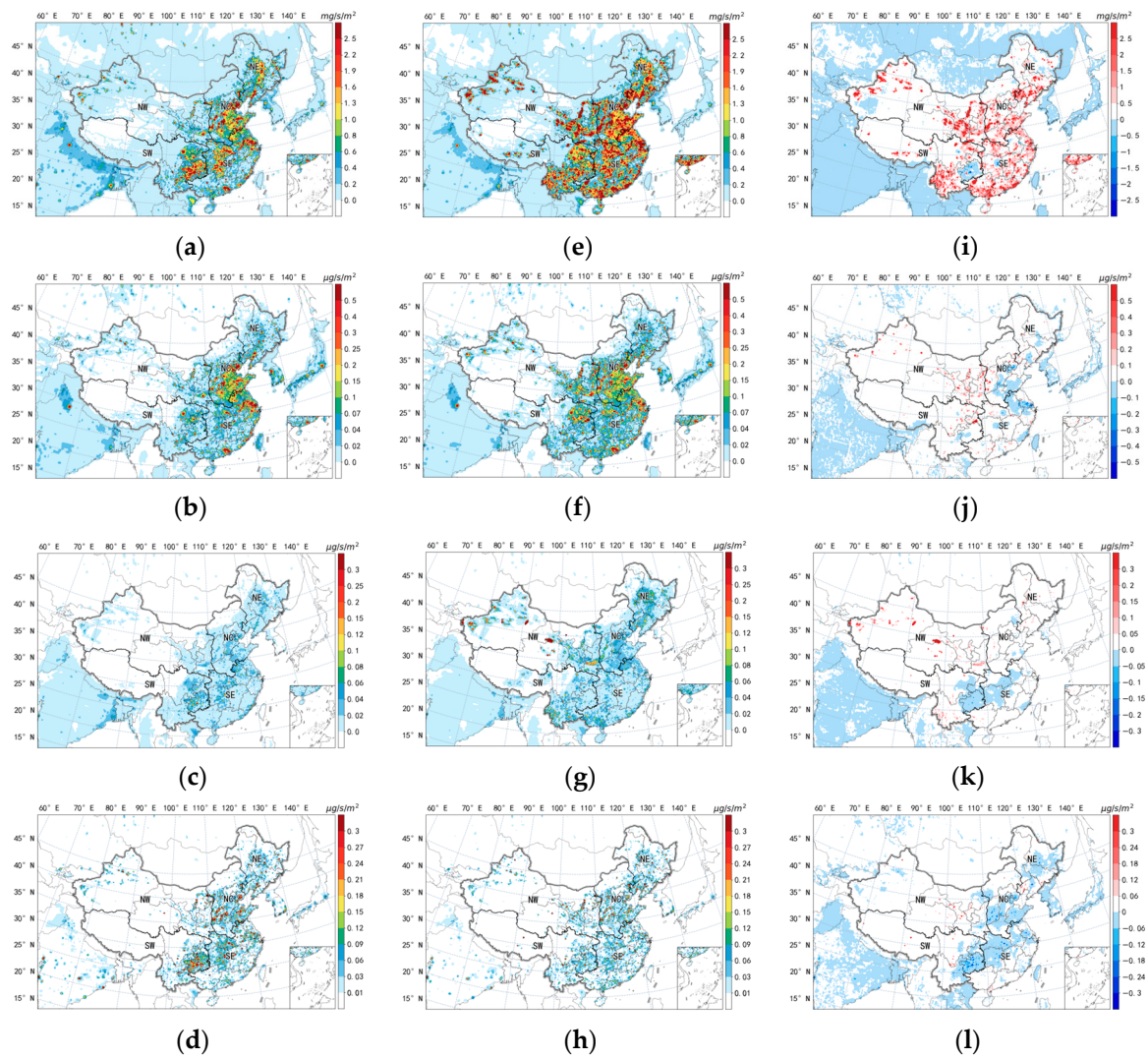


Figure 3. Distribution of CO, NO_x, OC, and SO₂ emission rates from different inventories: (a–d) priori emission inventory of CO, NO_x, OC, and SO₂; (e–h) updated emission inventory of CO, NO_x, OC, and SO₂; (i–l) differences in CO, NO_x, OC, and SO₂ emission rates before and after the inversion.

Table 1. Average emission rates of various pollutants across the country before and after inventory inversion of 2022 (unit: ng/s/m²).

Emission	Type	China	NE	NC	SE	NW	SW
PM _{2.5}	Priori	6.7	6.5	21.7	13.8	1.3	3.8
	Inversion	6.6	6.9	14.3	10.9	4.3	3.7
CO	Priori	297.3	339.4	641.8	632.9	77.1	221.4
	Inversion	702.4	689.5	1153.8	1442.2	388.6	482.0
NO _x	Priori	25.0	22.1	71.0	58.7	6.3	10.5
	Inversion	37.2	30.0	82.9	70.9	19.8	23.0
SO ₂	Priori	16.3	16.1	34.8	30.6	5.6	14.1
	Inversion	13.4	16.7	26.9	23.8	6.9	8.2
NMVOCs	Priori	45.6	35.9	109.5	124.6	7.9	23.2
	Inversion	40.3	39.2	106.3	92.0	11.7	17.0

Table 1. Cont.

Emission	Type	China	NE	NC	SE	NW	SW
BC	Priori	2.8	3.0	5.6	6.3	0.6	2.4
	Inversion	3.0	4.0	6.1	6.0	1.5	1.9
OC	Priori	5.6	6.0	9.0	13.0	1.4	5.2
	Inversion	10.5	15.4	15.6	13.6	7.2	6.0

3.2. PM_{2.5} Forecast Performance Analysis

Figure 4a presents the statistical results of PM_{2.5} concentration forecast accuracy for all cities in China. The forecast accuracy shows a decreasing trend with the increase in lead time. The inversion inventory improves the average accuracy rate of PM_{2.5} concentration forecasts by approximately 1.5–4.2% at different lead times. Among all the lead times, the accuracy rate for 1 d increases from 33.2% to 37.4%, with the largest improvement, followed by the accuracy rate for 2 d, which increases by 3.6%. The monthly distribution of the average accuracy rate for all cities nationwide is shown in Figure 4b, with significant improvements in the average accuracy rate for all the different lead times in the January–April and November–December periods, increasing by 7.0, 7.4, 10.3, 4.7, 1.8, and 4.7% in each respective month. By comparing the 1 d PM_{2.5} forecast concentration results, it can be observed that the monthly average concentrations and trends are overall closer to the observed results when using the updated inventory. It is noteworthy that in the months of January–March and November–December, which coincide with the heating season in most northern cities of China (from November to March each year), the observed monthly average PM_{2.5} concentrations are relatively higher. Numerous studies indicate that during the heating season, the significant increase in fossil fuel combustion can lead to a rise in PM_{2.5} concentrations in the atmosphere [22–24]. The improvement in PM_{2.5} concentrations with the updated inventory is more significant in the heating season compared to other periods.

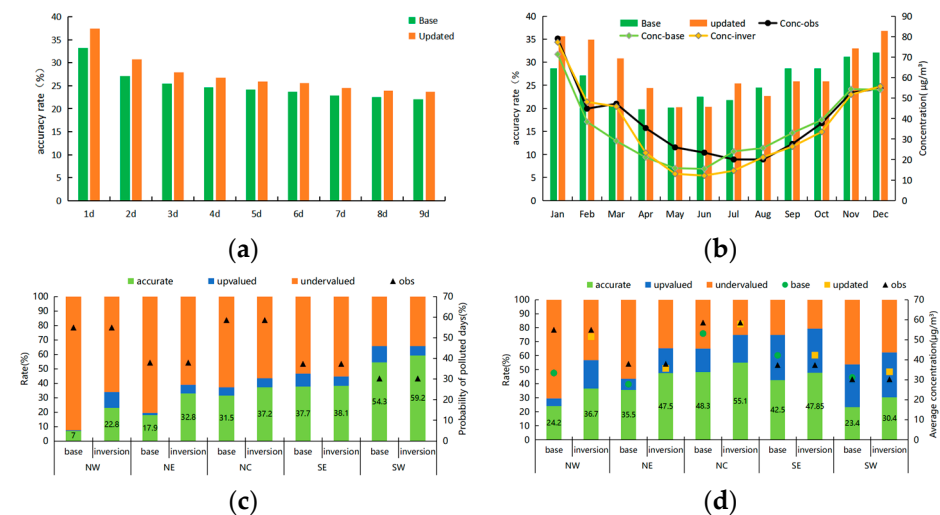


Figure 4. (a) Forecast accuracy of national PM_{2.5} concentration at different lead times; (b) primary axis: accuracy rate of PM_{2.5} forecast for all lead times, secondary axis: average concentration of 1 d PM_{2.5} and observation value in different months; (c) comparison of the forecast accuracy for pollution days at different lead times before and after inventory update in different regions; and (d) comparison of the forecast accuracy for the heating season at different lead times before and after inventory update in different regions.

When a day has an average PM_{2.5} concentration over 75 µg/m³, this day will be defined as a pollution day. After applying the inverted inventory, the average forecast accuracy of PM_{2.5} concentration for polluted days in Chinese cities increases from 31% to

38% for all the different lead times, especially for the 1 d forecast accuracy, which increases from 42.9% to 51.3%. Figure 4c compares the forecast results for different regions in China before and after the inventory update for the polluted days in 2022. The black triangle shown in Figure 4c represents the average probability of pollution days in the regions for the year of 2022, corresponding to the secondary axis. In the NE and NW regions, where emission rate adjustments are more significant in Section 3.1 after the inversion, the $PM_{2.5}$ forecast accuracy also improves significantly, increasing by 15.8% and 14.9%, respectively. The pollution probability in the NC region is comparable to that in the NW region and significantly higher than in the other regions, with a forecast accuracy increase of 5.7%. The SE and SW regions' forecast accuracy increases by 0.4% and 4.9%, respectively. In the SW region, which has the lowest pollution probability, the forecast accuracy of pollution days is relatively high compared to the other regions both before and after the inventory update. It is noteworthy that for all regions, the forecast bias of the baseline forecast is mainly underestimated. After the inventory update, the forecast bias slightly improves but remains primarily underestimated.

In order to reduce the impact of integration errors, the forecast result with the nearest lead time, which is 1 d, was selected for further analysis of the performance of the inverted inventory in forecasting $PM_{2.5}$ pollution events. Figure 4d compares the 1 d forecast performance before and after the inventory update during the heating season. The green circle, orange square, and black triangle represent the average $PM_{2.5}$ concentrations for the base forecast, updated forecast, and observation value during the heating season, respectively. It is noteworthy that the underestimation rates in the NE and NW regions were 70.3% and 56.3% before inventory update, respectively, and they significantly decreased to 41.2% and 34.6% after the update. The average $PM_{2.5}$ concentrations in the NW and NE regions were significantly underestimated in the base forecasts, and they became closer to the observation value after inventory update. In the NC region, the $PM_{2.5}$ concentration was slightly underestimated in base forecast, but after the update, it aligned closely with the observation value. Overall, there is a significant improvement in alleviating the underestimation situation in the forecasts during the heating season by applying the inventory inversion.

From 3 to 12 January 2022, a long-lasting and widespread $PM_{2.5}$ pollution event occurred in many cities in the NW, NC, and SE regions, reaching moderate to severe levels. The most severe pollution in the NC region was observed from the 8th to the 10th, and the distributions of $PM_{2.5}$ concentration forecasts and observation values are shown in Figure 5. In the figure, the shaded background represents the forecast results with a lead time of 1 d, while the filled colored dots indicate the observed results. Clearly, the forecast results of the priori inventory are significantly lower in the high-concentration pollution areas when comparing to the observation values. After applying the inverted inventory, the overall $PM_{2.5}$ concentration in the pollution areas shows a better match to the actual value, which means the forecast results of the inverted inventory are more accurate than those of the priori inventory.

The pollution events for the cities of Beijing (BJ), Tongchuan (TC), Shijiazhuang (SJZ), and Suqian (SQ) were selected to further analyze the performance of the inversion inventory, as shown in Figure 5. Beijing is located on the edge of the high-pollution area. After applying the inverted inventory, the forecast results for Beijing, Tongchuan, and Suqian were more consistent with the observed results. A comparison of the forecast concentrations and observed results before and after the inventory update for each city is shown in Figure 6. For Beijing, the RMSE decreased from 28.3 $\mu\text{g}/\text{m}^3$ to 13.1 $\mu\text{g}/\text{m}^3$, and the NMB improved from a high bias of 0.56 to a slightly low bias of 0.04. For Tongchuan, the RMSE decreased from 28.0 $\mu\text{g}/\text{m}^3$ to 15.1 $\mu\text{g}/\text{m}^3$, and the NMB improved from a low bias of 0.27 to a slightly low bias of 0.06. For Suqian, the RMSE decreased from 29.8 $\mu\text{g}/\text{m}^3$ to 20.6 $\mu\text{g}/\text{m}^3$, and the NMB decreased from 0.22 to -0.09 . All these results indicate an overall effective improvement for the forecast accuracy of the $PM_{2.5}$ concentration of these cities. However,

the forecast results for Shijiazhuang did not improve even after the inventory inversion; instead, there was a slight increase in bias for both the RMSE and NMB indicators.

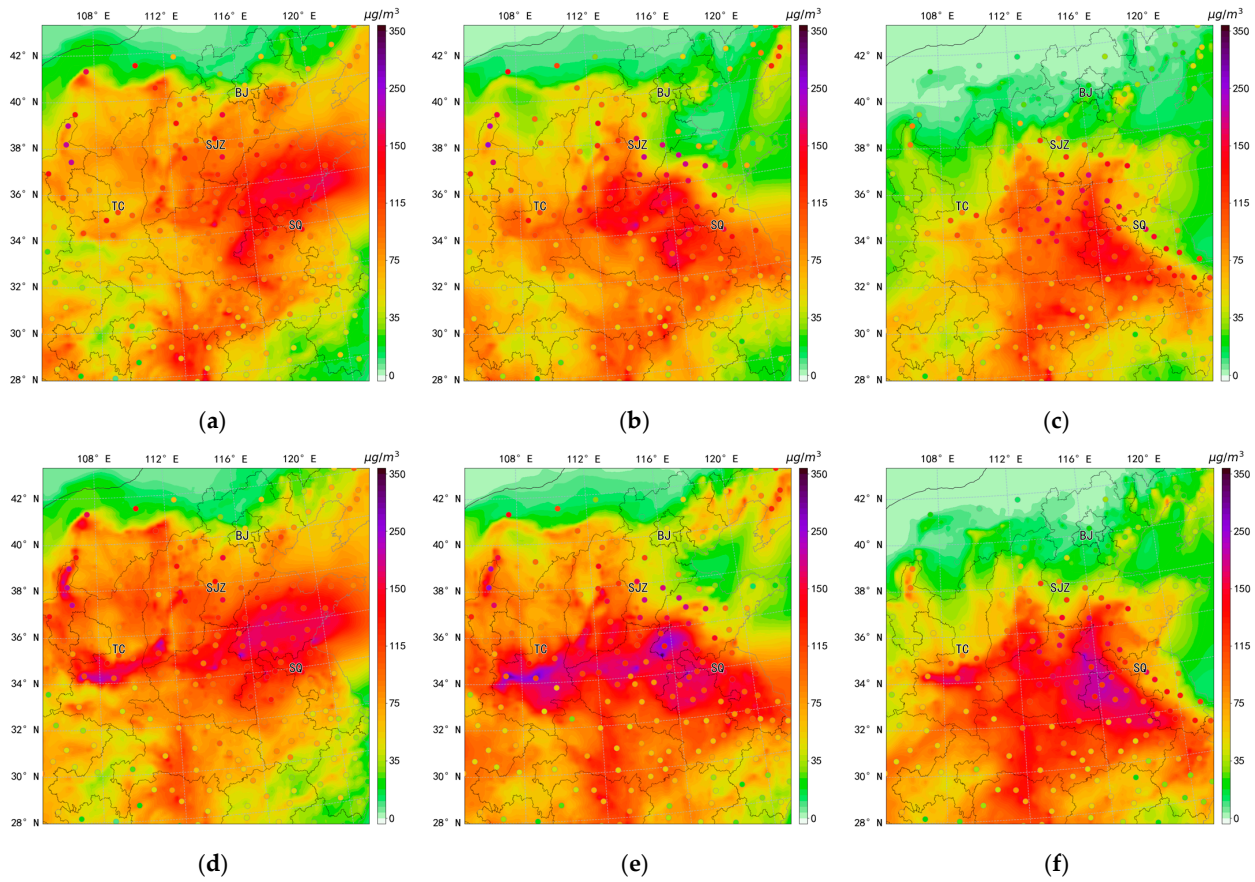


Figure 5. Comparison of $PM_{2.5}$ forecast results and monitoring results before (a–c) and after (d–f) the inversion during 8th–10th January (shaded background: the forecast results with a lead time of 1 d; filled colored dots: the observed results).

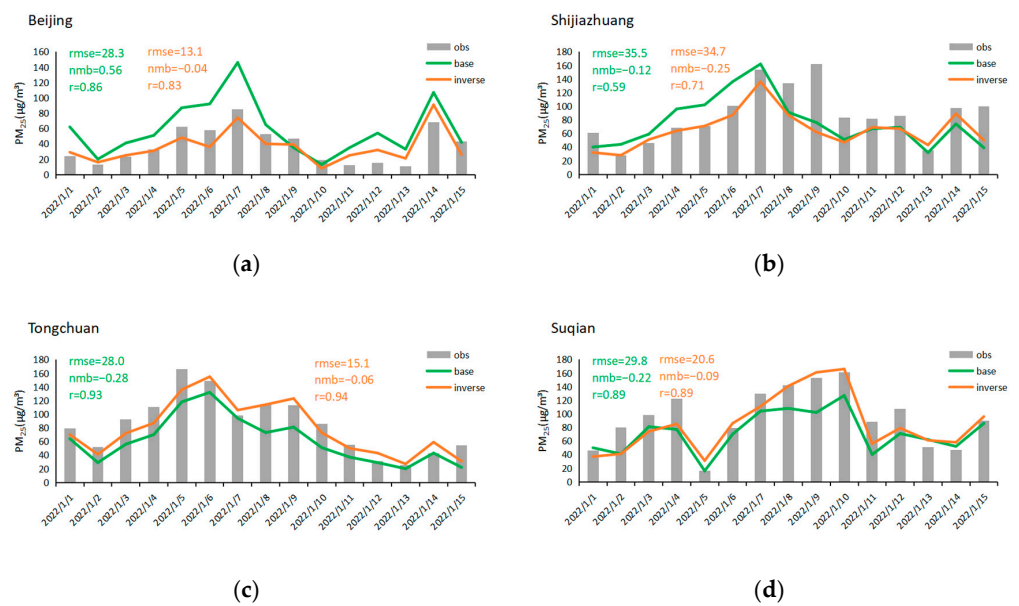


Figure 6. Daily $PM_{2.5}$ concentration of (a) Beijing, (b) Shijiazhuang, (c) Tongchuan, and (d) Suqian during 1st–15th January (green line: base; orange line: inversion; grey column: observation).

Figure 7 shows the hourly forecast performance of particulate matter components in Shijiazhuang. It can be observed that secondary particulate matter components such as sulfate, nitrate, and ammonium were significantly underestimated from the 8th to the 10th of the month after inversion. Previous studies [25,26] have also indicated that the lack of key mechanisms for the rapid growth of pollution in the autumn and winter seasons in the NC region can lead to an underestimation of secondary particulate matter components in air quality numerical models. As shown in Figure 6, after updating the inversion inventory, the daily average total PM_{2.5} concentration on pollution days in the representative cities still tends to be underestimated. This underestimation is particularly prominent in Shijiazhuang. The mean PM_{2.5} concentration from the 8th to the 10th of the month decreased by 24 $\mu\text{g}/\text{m}^3$ in the inversion inventory compared to the baseline inventory, resulting in a value that was 55% lower compared to monitoring data. However, when examining the hourly concentration of the primary component BC in Figure 7, it can be observed that the simulation results match the monitored BC concentration better after applying the inverted inventory. Therefore, conducting simulations based on the inverted emission inventory allows for a better representation of particulate matter component concentrations. In addition, for pollutants, especially secondary pollutants, simulation discrepancies may arise from factors such as emission inventory and chemical reaction mechanisms. The inverted inventory can reduce the simulation discrepancies introduced by the emission inventory, identify the sources of simulation uncertainties, and subsequently carry out targeted updates of mechanisms to improve model simulation performance.

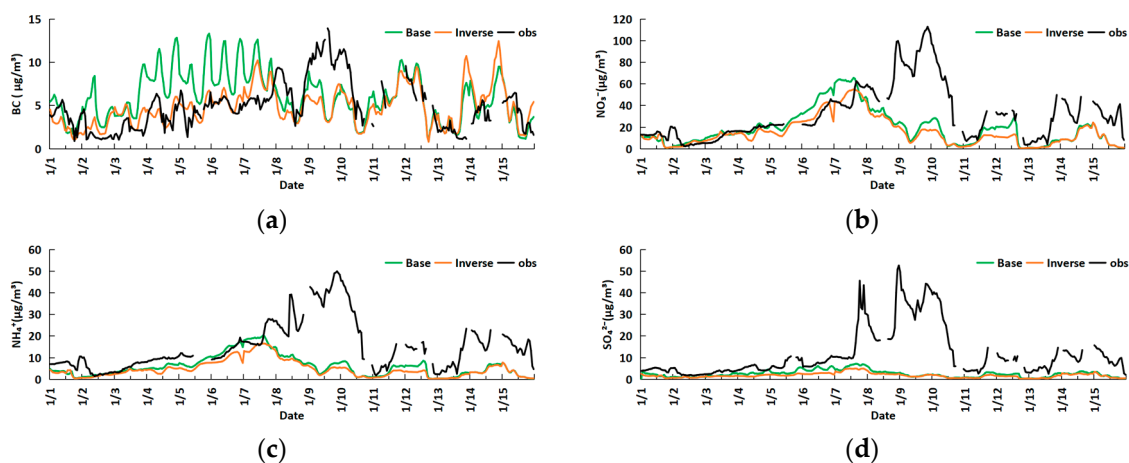


Figure 7. Concentrations of (a) BC, (b) NO_3^- , (c) NH_4^+ , and (d) SO_4^{2-} in city of Shijiazhuang (green line: base; orange line: inversion; black line: observation).

4. Conclusions

In this paper, we employed an inversion system based on EnKF to invert the emission inventory of 2022 in China. We used the inverted inventory to continuously update the input data for the forecasting system, enabling the daily prediction of PM_{2.5} concentration for the next 9 days. A comprehensive evaluation of the PM_{2.5} forecast performance before and after the inventory updates was conducted to analyze the impact and shortcomings of the inventory updates on PM_{2.5} concentration forecasting. The overall conclusions are as follows:

- (1) After the inversion, adjustments were applied to the emission rates of various pollutants, with significant increases in CO, NO_x, and OC emission rates and a notable decrease in SO₂ emission rates. The NE and NW regions showed more pronounced adjustments in emission rates for various pollutants compared to other regions in China.
- (2) In comparison to the forecast results based on the priori emission inventory, the forecast accuracy of PM_{2.5} concentration for different lead times improved after applying the updated inventory, especially the accuracy of the 1–3 d forecasts, which increased by 2.5–4.2%. Meanwhile, the forecast accuracy during the heating season significantly

improved compared to other months, with an average monthly increase of approximately 6.3% after the inventory inversion. The improvement in the accuracy of pollution day forecasts is beneficial for proposing more precise control measures. The overall forecast accuracy in the NE and NW regions showed particularly significant improvement on pollution days. The forecast performance for the pollution event from the NC region in early January 2022 was notably enhanced with the use of the inverted emission inventory, addressing the underestimation issues present in the priori inventory during this period.

- (3) While emission inventory inversion can improve the forecast accuracy to a certain extent, underestimation issues persisted, especially in the prediction of secondary particulate matter. Future improvements can be made by utilizing more observation data, such as particle components, to invert and enhance the emission source inventory for secondary particulate matter precursors. To further improve the forecast performance of pollutants, it is very necessary to improve the chemical reaction mechanism in this model, because the underestimation issue may be related to it.

Author Contributions: Conceptualization, X.T. and L.C.; methodology, L.K. and H.W.; investigation, W.Y.; visualization, Y.Z.; writing—original draft preparation, L.Z.; writing—review and editing, M.F. and C.Y. All authors have read and agreed to the published version of the manuscript.

Funding: This research was funded by the National Key Research and Development Program of China (Grant No. 2021YFB3901000) and the National Natural Science Foundation of China (Grant No. 41830109).

Data Availability Statement: The data presented in this study are available on request from the corresponding author. The data are not publicly available due to the size of the dataset.

Conflicts of Interest: Author Yao Zhao is employed by the company 3Clear Technology Co., Ltd. The paper reflects the views of the scientists and not the company. The authors declare no conflicts of interest.

References

1. Wang, Z.; Pang, C.; Zhu, J. IAP Progress in atmospheric environment modeling research. *Chin. J. Atmos. Sci.* **2008**, *32*, 987–995.
2. Brasseur, G.P.; Jacob, D. *Modeling of Atmospheric Chemistry*; Cambridge University Press: Cambridge, UK, 2017; pp. 399–435.
3. Hayami, H.; Sakurai, T.; Han, Z.; Ueda, H.; Carmichael, G.R.; Streets, D.; Holloway, T.; Wang, Z. MICS-Asia II: Model intercomparison and evaluation of particulate sulfate, nitrate and ammonium. *Atmos. Environ.* **2008**, *42*, 3510–3527. [[CrossRef](#)]
4. Carmichael, G.; Sakurai, T.; Streets, D.; Hozumi, Y.; Ueda, H.; Park, S.; Fung, C.; Han, Z.; Kajino, M.; Engardt, M.; et al. MICS-Asia II: The model intercomparison study for Asia Phase II methodology and overview of findings. *Atmos. Environ.* **2008**, *42*, 3468–3490. [[CrossRef](#)]
5. Hanna, S.R.; Chang, J.C.; Fernau, M.E. Monte Carlo estimates of uncertainties in predictions by a photochemical grid model (UAM-IV) due to uncertainties in input variables. *Atmos. Environ.* **1998**, *32*, 3619–3628. [[CrossRef](#)]
6. Yang, W.; Li, J.; Zhu, L.; Wang, Z. Comparison of anthropogenic emission inventories of China mainland. *Res. Environ. Sci.* **2013**, *26*, 703–711.
7. Saikawa, E.; Kim, H.; Zhong, M.; Avramov, A.; Zhao, Y.; Janssens-Maenhout, G.; Kurokawa, I.; Klimont, Z.; Wagner, F.; Naik, V.; et al. Comparison of emissions inventories of anthropogenic air pollutants and greenhouse gases in China. *Atmos. Chem. Phys.* **2017**, *17*, 6393–6421.
8. Zhang, L.; Zhao, T.; Gong, S.; Kong, S.; Tang, L.; Liu, D.; Wang, Y.; Jin, L.; Shan, Y.; Tan, C.; et al. Updated emission inventories of power plants in simulating air quality during haze periods over East China. *Atmos. Chem. Phys.* **2018**, *18*, 2065–2079. [[CrossRef](#)]
9. Miyazaki, K.; Eskes, H.J.; Sudo, K.; Takigawa, M.; Van Weele, M.; Boersma, K.F. Simultaneous assimilation of satellite NO₂, O₃, CO, and HNO₃ data for the analysis of tropospheric chemical composition and emissions. *Atmos. Chem. Phys.* **2012**, *12*, 9545–9579. [[CrossRef](#)]
10. Peng, Z.; Lei, L.; Liu, Z.; Sun, J.; Ding, A.; Ban, J.; Chen, D.; Kou, X.; Chu, K. The impact of multi-species surface chemical observation assimilation on air quality forecasts in China. *Atmos. Chem. Phys.* **2018**, *18*, 17387–17404. [[CrossRef](#)]
11. Feng, S.; Jiang, F.; Jiang, Z.; Wang, H.; Cai, Z.; Zhang, L. Impact of 3DVAR assimilation of surface PM 2.5 observations on PM 2.5 forecasts over China during wintertime. *Atmos. Environ.* **2018**, *187*, 34–49. [[CrossRef](#)]
12. Wu, H.; Kong, L.; Tang, X.; Zhu, L.; Zhu, J.; Wang, Z. Air Quality Forecasting with Inversely Updated Emissions for China. *Environ. Sci. Technol. Lett.* **2023**, *10*, 655–661. [[CrossRef](#)]
13. Li, M.; Liu, H.; Geng, G.; Hong, C.; Liu, F.; Song, Y.; Tong, D.; Zheng, B.; Cui, H.; Man, H.; et al. Anthropogenic emission inventories in China: A review. *Natl. Sci. Rev.* **2017**, *4*, 834–866. [[CrossRef](#)]

14. Zheng, B.; Tong, D.; Li, M.; Liu, F.; Hong, C.; Geng, G.; Li, H.; Li, X.; Peng, L.; Qi, J.; et al. Trends in China's anthropogenic emissions since 2010 as the consequence of clean air actions. *Atmos. Chem. Phys.* **2018**, *18*, 14095–14111. [[CrossRef](#)]
15. MEICmodel. Available online: <http://www.meicmodel.org/> (accessed on 1 November 2021).
16. Li, M.; Zhang, Q.; Kurokawa, J.; Woo, J.-H.; He, K.; Lu, Z.; Ohara, T.; Song, Y.; Streets, D.G.; Carmichael, G.R.; et al. MIX: A mosaic Asian anthropogenic emission inventory under the international collaboration framework of the MICS-Asia and HTAP. *Atmos. Chem. Phys.* **2017**, *17*, 935–963. [[CrossRef](#)]
17. Zhang, Q.; Streets, D.G.; Carmichael, G.R.; He, K.B.; Huo, H.; Kannari, A.; Klimont, Z.; Park, I.S.; Reddy, S.; Fu, J.S.; et al. Asian emissions in 2006 for the NASA INTEX-B mission. *Atmos. Chem. Phys.* **2009**, *9*, 5131–5153. [[CrossRef](#)]
18. Streets, D.G.; Bond, T.C.; Carmichael, G.R.; Fernandes, S.D.; Fu, Q.; He, D.; Klimont, Z.; Nelson, S.M.; Tsai, N.Y.; Wang, M.Q.; et al. An inventory of gaseous and primary aerosol emissions in Asia in the year 2000. *J. Geophys. Res. Atmos.* **2003**, *108*, 23. [[CrossRef](#)]
19. Evensen, G. Sequential data assimilation with a nonlinear quasi-geostrophic model using Monte Carlo methods to forecast error statistics. *J. Geophys. Res. Ocean.* **1994**, *99*, 10143–10162. [[CrossRef](#)]
20. Wang, Z.; Maeda, T.; Hayashi, M.; Hsiao, L.F.; Liu, K.Y. A nested air quality prediction modeling system for urban and regional scales: Application for high-ozone episode in Taiwan. *Water Air Soil Pollut.* **2001**, *130*, 391–396. [[CrossRef](#)]
21. Kong, L.; Tang, X.; Zhu, J.; Wang, Z.; Pan, Y.; Wu, H.; Wu, L.; Wu, Q.; He, Y.; Tian, S.; et al. Improved inversion of monthly ammonia emissions in China based on the Chinese ammonia monitoring network and ensemble Kalman filter. *Environ. Sci. Technol.* **2019**, *53*, 12529–12538. [[CrossRef](#)]
22. Xiao, Q.; Ma, Z.; Li, S.; Liu, Y. The impact of winter heating on air pollution in China. *PLoS ONE* **2015**, *10*, e0117311. [[CrossRef](#)]
23. Wang, S.; Li, Y.; Haque, M. Evidence on the Impact of Winter Heating Policy on Air Pollution and Its Dynamic Changes in North China. *Sustainability* **2019**, *11*, 2728. [[CrossRef](#)]
24. Liang, B.; Li, X.; Ma, K.; Liang, S.-X. Pollution characteristics of metal pollutants in PM 2.5 and comparison of risk on human health in heating and non-heating seasons in Baoding, China. *Ecotoxicol. Environ. Saf.* **2019**, *170*, 166–171. [[CrossRef](#)]
25. Wang, W.; Liu, M.; Wang, T.; Song, Y.; Zhou, L.; Cao, J.; Hu, J.; Tang, G.; Chen, Z.; Li, Z.; et al. Sulfate formation is dominated by manganese-catalyzed oxidation of SO₂ on aerosol surfaces during haze events. *Nat. Commun.* **2021**, *12*, 1993. [[CrossRef](#)] [[PubMed](#)]
26. Huang, C.; Ma, C.; Wang, T.; Qu, Y.; Li, M.; Li, S.; Zhuang, B.; Xie, M. Study on the assimilation of the sulphate reaction rates based on WRF-Chem/DART. *Sci. China Earth Sci.* **2023**, *66*, 2239–2253. [[CrossRef](#)]

Disclaimer/Publisher's Note: The statements, opinions and data contained in all publications are solely those of the individual author(s) and contributor(s) and not of MDPI and/or the editor(s). MDPI and/or the editor(s) disclaim responsibility for any injury to people or property resulting from any ideas, methods, instructions or products referred to in the content.